**ACADEMIA JOURNAL OF BIOLOGY** 2025, 47(2): 17–32
DOI: 10.15625/2615-9023/22551

# MUTATION OF YEAST *PEX6* GENE INHIBITS GLYCOLYSIS AND MITOCHONDRIAL RESPIRATORY CHAIN BUT PROMOTES GLYCOGEN AND TREHALOSE BIOSYNTHESIS AND NECROSIS

**Van Ngoc Bui[1,2,*], Hoang Ha Chu[1,2]**

[1]Institute of Biology, Vietnam Academy of Science and Technology, 18 Hoang Quoc Viet, Ha Noi, Vietnam
[2]Graduate University of Science and Technology, Vietnam Academy of Science and Technology, 18 Hoang Quoc Viet, Ha Noi, Vietnam

Received 13 March; accepted 4 June 2025

## ABSTRACT

In yeast, Pex6 (peroxisomal biogenesis factor 6) encoded by the *PEX6* gene plays a crucial role in peroxisomal protein import, cell viability, and necrosis. Moreover, the activity of some key glycolytic enzymes is changed due to DNA damage or oxidative stress, leading to the diversion of metabolic flux into other biochemical pathways, such as the pentose phosphate pathway (PPP), hexosamine biosynthesis pathway (HBP), and glycogen and trehalose synthesis.

Thus, the present study aims to examine the role of the *PEX6* gene by using the BY4741 (wild type) and specific knock-out yeast strains (Δ*pex6*). The activity of this gene in these biochemical pathways in response to DNA damage triggered by methyl methanesulfonate (MMS) treatment would be elucidated by using enzymatic, Gloxo, and OxoPlate® assays, flow cytometry, and chromatography.

The findings obtained show that DNA damage significantly inhibited the activity of glyceraldehyde-3-phosphate dehydrogenase (GAPDH) and pyruvate kinase (PYK), mitochondrial respiration, cell growth, and ATP synthesis. However, DNA damage intensively promotes the activity of glucose-6-phosphate dehydrogenase (G6PDH) and the synthesis of uridine-diphosphoglucose-N-acetylglucosamine (UDP-NacGlu). Subsequently, the glucose flux was not diverted to the TCA cycle due to prohibited mitochondrial activity and oxygen consumption, but to the PPP as a result of increased G6PDH activity and to glycogen/trehalose accumulation because of enhanced UDP-NacGlu levels. The cells, especially the mutant Δ*pex6*, utilize glycogen/trehalose as major energy reserves to maintain their energy and survival, and induce necrosis as a cellular defense mechanism in response to DNA damage. These results suggest that a fully functional *PEX6* plays a major role in cell proliferation, energy metabolism, and the cellular defense mechanism in response to DNA damage.

**Keywords:** DNA damage, glycolytic enzyme, glycogen, mitochondria, necrosis, trehalose, PEX6.

*Citation*: Van Ngoc Bui, Hoang Ha Chu, 2025. Mutation of yeast *PEX6* gene inhibits glycolysis and mitochondrial respiratory chain but promotes glycogen and trehalose biosynthesis and necrosis. *Academia Journal of Biology*, 47(2): 17–32. https://doi.org/10.15625/2615-9023/22551

[*]*Corresponding author email*: bui@ibt.ac.vn

## INTRODUCTION

In budding yeast *Saccharomyces cerevisiae*, Pex6 (peroxisomal biogenesis factor 6) is a peroxin encoded by *PEX6* gene and a peroxisomal membrane protein involved in peroxisomal protein import (Ali et al., 2023; Rüttermann et al., 2023). Pex6 acts downstream of the receptor docking in the terminal steps of peroxisomal matrix protein import (Grimm et al., 2012). Also, Pex6 is supposed to control ROS accumulation (Min et al., 2012) and cell viability in the early stationary phase, and it does not depend on the apoptotic activators Yca1 (yeast caspase 1) and Aif1 (apoptosis inducing factor) in apoptosis, but triggers necrotic cell death (Jungwirth et al., 2008). Thus, deficiency in *PEX6* should lead to loss of cell viability and cause necrosis. In humans, mutations in *PEX6* can lead to severe peroxisomal disorders and early death (Ebberink et al., 2010; Lucaccioni et al., 2020; Renaud et al., 2016) and disruption of the *PEX1-PEX6* interaction often causes the neurological disorders such asZellweger syndrome (Geisbrecht et al., 1998).

In eukaryotic cells, many studies indicating the role of some key glycolytic enzymes in oxidative stress and apoptosis have been reported (Cerella et al., 2009; Matte et al., 2021; Muronetz et al., 2020; Wang et al., 2017). Those enzymes are including glucose 6-phosphate dehydrogenase (G6PDH) (Sousa et al., 2020; Ueda et al., 2018), glyceraldehyde-3-phosphate dehydro-genase (GAPDH) (Christodoulou et al., 2018; Hildebrandt et al., 2015), and pyruvate kinase (PYK) (Grüning et al., 2011; Shimizu & Matsuoka, 2019), whose activity is altered upon DNA damage or oxidative stress induced by exogenous or endogenous agents, leading to subsequent alterations of metabolic flux. However, to date, no study has examined the role of yeast G6PDH, GAPDH, and PYK in the oxidative defence systems or apoptosis and their role in the energy metabolism and metabolic alterations in response to oxidative stress/DNA damage.

It is well known that *S. cerevisiae* has long been recognized as a versatile model system for drug discovery and studying of cellular defense in eukaryotic cells, since many of the basic cellular processes of both yeast and humans are also highly conserved. Thus, the purpose of this study is to investigate the role of *PEX6* in glycolysis, energy metabolism, metabolic alterations, namely carbohydrate flux to the hexosamine and pentose phosphate pathways or glycogen and trehalose synthesis, and necrosis (apoptosis). The present study, therefore, uses the model yeast strain BY4741 (wild type) and the mutant Δ*pex6* that is defective in *PEX6* gene deleted by the disruption of the respective gene to test these biochemical pathways.

## MATERIALS AND METHODS

### Strains, media and growth conditions

Two yeast strains *S. cerevisiae* used in this study are the BY4741 wild type (Accession number: Y00000; Genotype: *MATα; his3Δ1; leu2Δ0; lys2Δ0; ura3Δ0*; Source: EUROSCARF) and the mutant Δ*pex6* (Accession number: Y01115; Genotype: *MATα; his3Δ1; leu2Δ0; lys2Δ0; ura3Δ0; YNL329c:kanMX4*; Source: EUROSCARF). Yeast cells were grown in rich medium (YPD, Yeast Peptone Dextrose) containing 10 g/L yeast extract, 20 g/L bacto peptone, and 20 g/L glucose. Cell growth was followed by optical absorbance measurement at 600 nm ($OD_{600}$). For treatment with DNA-damaging agents, e.g. methyl methanesulfonate (MMS), the medium was inoculated with an overnight preculture and grown at 30 ˚C to the mid-log phase ($OD_{600}$ 0.6–0.8). Then, cultures were either nontreated (control) or treated with different concentrations of MMS (Sigma-Aldrich). Yeast cells were first inoculated in YPD medium, incubated at 30 ºC/250 rpm/overnight (pre-culture), then pre-culture was transferred in fresh respective media YPD (main culture).

### Enzymatic Assay

The Enzymatic Assay was used to determine the activity of glycolytic enzymes. In this research, it was applied to determine two Michaelis Menten constants, such as $V_{max}$ and $K_m$ of glycealdehyde-3-phosphate

dehydrogenase (GAPDH, EC 1.2.1.12), pyruvate kinase (PYK, EC 2.7.1.40), and glucose-6-phosphate dehydrogenase (G6PDH, EC 1.1.1.49).

*Protein isolation*: The main culture was divided in two, one half culture as control (non-treated), another one was treated with 0.03% MMS. Aliquots (ca 20 $OD_{600}$ units of cells) were taken at 4 h and 24 h, centrifuged at 7,000 rpm/4 ºC/3 min. Pellets were resuspended with 1 g glass beads and 500 µL of Extraction Buffer (20 mM Hepes pH 7.1, 100 mM KCl, 5 mM EDTA pH 8, 1 mM DTT, and 0.1% Tween). Samples were vortexed twice for 5 mininutes, with cooling on ice in between, freezed at -20 ºC/overnight, and 1x5 min in Mixer Mill MMS 300 (Retsch). Broken cell suspensions were centrifuged at 13,000 rpm/4 ºC/20 min, supernatants (cell lysates) were immediately used for enzymatic assay to determine individual enzyme activity ($V_{max}$) and $K_m$, concomitantly used for determination of protein content by Bradford method.

*Assay execution*: The method followed the protocol as described in our previous reports (Bonowski et al., 2010; Kitanovic et al., 2009). Briefly, GAPDH activity was measured at 30 ºC by coupling the production of glycerate-1,3-diphosphate from 3-phosphoglyceric acid to the consumption of NADH, using a spectrophotometric assay in a coupled 3-phosphoglyceric phosphokinase-GAPDH system. PYK activity was measured at 30 ºC by coupling the production of pyruvate from phospho(enol)-pyruvate and ADP to the consumption of NADH, using a spectrophotometric assay in a coupled PYK-lactic dehydrogenase system. The reactions were initiated by the addition of crude extract and were followed by a decrease in $A_{340}$ nm.

*Data analysis*: $V_{max}$ and $K_m$ were determined from enzyme activities at different substrate concentrations [*S*]. R function *nls* (nonlinear least squares) was used to perform a direct nonlinear regression of the Michaelis Menten formula to determine these constants (Bonowski et al., 2010). The data were then saved in RData files and analyzed by the R program. The final results were plotted in R graphs that represent the kinetic curves of Michaelis Menten constants performing the relationship between $V_{max}$ and $K_m$ values. Finally, $V_{max}$ and $K_m$ values were represented in bar diagrams.

**Detection of mitochondrial activity and apoptosis by flow cytometry**

*Preparation*: The main culture was split in two, one half culture as control (non-treated), another one was treated with 0.03% MMS. Aliquots (ca 50–100 µL) were taken at 3 hours (h), 6 h, 8 h and 24 h after MMS treatment and mixed with ca 900 µL PBS (ca 1 mL total). Aliquots were stained with 1 µM MitoTracker® Green FM (Molecular Probes - in f.c) plus 5 µg/mL of propidium iodide (PI, Sigma-Aldrich, in f.c) for mitochondrial activity detection. For apoptosis analysis, the annexin V/PI staining assay (BD Biosciences, Germany) was used to analyze cell apoptosis according to the protocol of manufacturer. Living cells were determined as cells negative for both V and PI (V−/PI−), early apoptosis as cells positive for annexin V but negative for PI (V+/PI−), late apoptosis as cells positive for both annexin V and PI (V+/PI+), and necrotic cells as cells negative for V but positive for PI (V−/PI+). An aliquote of the resuspended cells was used to determine the cell number after treatment, using a hemocytometer and trypan blue. The relative amount of cells was calculated as the number of trypan blue negative cells divided by the number in the mock treatment (Bui et al., 2024).

*Flow cytometry analysis (FACS)*: FACS® Calibur (Becton Dickinson) and CellQuest Pro analysis software were used to quantify and analyzed fluorescence intensity of DHE, PI-DNA complex (excitation and emission settings were 488 and 564–606 nm, FL2 filter), and MitoTracker® (excitation and emission settings were 488 and 525–550 nm, FL1 filter). The analyzed fluorescence signal was given in the mean value of fluorescence intensity at the indicated time point (time course).

**OxoPlate® Assay**

OxoPlate® (PreSens, Germany) was used to monitor oxygen consumption of cell growth

in a medium. Yeast cells were first inoculated in YPD medium, incubated at 30 ºC/250 rpm/overnight (pre-culture), then pre-culture was transferred in fresh respective media YPD (main culture). Oxygen consumption (%) and cell growth ($OD6_{00}$) were monitored in 96-well OxoPlate® with round bottom integrated optical oxygen sensors, in which each well contained 75 µL of adjusted main culture (0.1 $OD_{600}$) and 75 µL of MMS with investigated concentration (i.e. 150 µL total).

The OxoPlate® was sealed with a breathable membrane (Diversified Biotech, USA), then introduced to Tecan Safire$^2$ Reader (Tecan, Switzerland) to measure fluorescence intensity at 540/650 nm (for indicator dye, $I_{indicator}$) and 540/590 nm (for reference dye, $I_{reference}$), and at 600 nm (for optical density of culture, $OD_{600}$). Measurement were carried out continuously over 18 h with a kinetic interval of 30 min at 30 ºC. The calibration of the fluorescence reader was performed using a two-point calibration curve with oxygen free water (80 mM $Na_2SO_3$, *Cal 0*) and air-saturated water (*Cal 100*). The partial pressure of oxygen was calculated from the calibration curve.

**Analysis of metabolite contents by high performance ion exchange chromatography (HPIC)**

*Metabolite extraction and sample preparation*: The sampling preparation was described previously (Loret et al., 2007). Briefly, 20 units $OD_{600}$ of cell culture were withdrawn at the indicated time point, rapidly collected by vacuum filtration (Glass Filter, Millipore™) through a Sartolon polyamide membrane (Sartorius, Germany). The cell-adherent membrane was quenched in 5 mL buffered ethanol (75% ethanol, 10 mM Hepes, pH 7.1) in a 50 mL-glass tube (Lenz, Laborglas- instruments, Germany), shortly vortexed, incubated at 85 ºC/4 min in water bath, and immediately put on ice. The membrane was then washed 2 × 0.5 mL with absolute ethanol to rinse the rest on the membrane in the solvent. The solvent containing cell extract suspension was evaporated to dryness at 35–40 ºC under a vacuum rotary around 35–50 mbar (Büchi, Rotavapor R, Switzerland). Cell extract was resuspended in 0.5 mL deionized water, centrifuged at 13000 rpm/4ºC/5 min. The supernatant was introduced to HPIC for analysis.

*Analysis of nucleotide content*: Supernatants (ca 200 µL) were transferred into 1.5 mL-screw thread vials with glass inserts (VWR™) and analyzed by High Performance Ion Exchange Chromatography (HPIC, Dionex - ICS - 3000, USA) equipped with gradient pump and conductivity detector along with UV detector (wavelength was set either to 220 or 260 nm). For the chromatographic separation, an AG11 guard column (50 mm × 2 mm i.d.) and 2 AS11 analytical columns (250 mm × 2 mm i.d.) (Dionex) in series were used. A flow of 0.35 mL/min was maintained throughout all runs. The suppressor current was set to 70 mA. The sample injection volume was 5 µL. The data was analyzed by Chromeleon software (Dionex, ICS - U3000). The content of metabolites and nucleotides was then analyzed by Chromeleon software based on the calibration curve to quantify ATP and UDP-NAcGlu contents, and calculated in µmol/g DW (dry weight). The analytical protocol follows the method described by Ritter (2006) (Ritter et al., 2006).

**Gloxo Assay (glucose oxidase method)**

Gloxo Assay is used to monitor the glucose consumption of cells during cultivation. Yeast cells were inoculated in YPD medium, incubated at 30 ºC/250 rpm/overnight (pre-culture), then the pre-culture was transferred in fresh YPD medium, and incubated at 30 ºC/250 rpm until mid-log phase (main culture). The main culture was divided, one half of which was used as control (non-treated), and the other treated with 0.03% MMS. After MMS treatment, aliquots (ca 20 units $OD_{600}$ of cell culture) were withdrawn every hour till 48 h. Cell cultures were centrifuged at 3600 rpm/4 ºC/5 min. The

supernatants were introduced to Gloxo Assay to determine the glucose concentration in the medium, the pellets were used for quantitative analysis of glycogen and trehalose by Glycogen and Trehalose Assay. The principle of Gloxo Assay is that glucose oxidase enzyme (EC 1.1.3.4) catalyzes the oxidation of glucose in the medium into D-glucono-1,5-lactone which then hydrolyzes to gluconic acid, simultaneously oxygen is reduced to hydrogen peroxide. The supernatants (culture media) in 1.5 mL Eppendorf tubes, Gloxo Reagent (Tris-Cl 250 mM pH 8, glucose oxidase 250 µg/mL, peroxidase 100 µg/mL, reduced-o-dianisidine 100 µg/ mL prepared in absolute ethanol), standard glucose solutions (0, 1, 2, 4 µg/mL), and deionized water were manually prepared. Quantitative analysis of glucose concentration in the medium based on the calibration curve. Glucose consumption at each time point was calculated in g/L medium.

**Glycogen and Trehalose Assay**

The pellets collected from Gloxo Assay were then resuspended in 250 µL of $Na_2CO_3$, incubated in water bath at 95 ºC/4 h, put on ice. The broken cell suspension was adjusted to pH 5.2 by adding 150 µL of 1M acetic acid and 600 µL of 0.2 M sodium acetate buffer and divided in two. One half (500 µL) was with 100 µg of α-amyloglucosidase from *Aspergillus niger*, incubated overnight at 57 $^{o}$C/in Thermomixer (Eppendorf, Germany) with continuous shaking ca 800 rpm. Another half was added with 3 mU trehalase, incubated overnight at 37 $^{o}$C in Thermomixer with continuous shaking ca 800 rpm.

The overnight incubated suspensions were centrifuged at 13,000 rpm/4 ºC/5 min, the supernatants containing released glucose molecules were introduced to Gloxo Assay as described above to determine glucose concentration. The data were analyzed, glycogen and trehalose contents were calculated in mg glucose/g DW (dry weight). The final results were performed in graphs that represented the correlation of the kinetics of glycogen and trehalose accumulation to glucose consumption in the medium.

**Statistical data analysis**

Values were taken as means of three determinations. The differences between the means were determined by Duncan's Multiple Range Test (MRT) using SAS 9.0 software (SAS Institute, Cary, NC, USA) and means with the same letter were not significantly different ($p > 0.05$). Also, one-way ANOVA Kruskal–Wallis test was performed to determine differences in distributions between two or more independent groups using the *kruskal.test* function in R, $p$-values < 0.05 were considered to be significantly different.

**RESULTS**

**Changes in activity of glycolytic enzymes upon MMS treatment**

MMS treatment strongly decreased GAPDH activity of both strains from as early as 4 hours and up to 24 hours (h). Especially, GAPDH activity in all cells was suppressed after 24 hours of treatment (Figs. 1A–B). Similar to GAPDH, PYK activity of all strains was strongly inhibited from 4–24 hours upon MMS treatment and was not able to recover (Figs. 1C–D). The GAPDH and PYK activities of the mutant Δ*pex6* cells were comparatively lower than those of the wild type BY4741 upon treatment with or without MMS (Figs. 1A–D).

In contrast to GAPDH and PYK, G6PDH activity of all strains was not inhibited by MMS treatment at all. In fact, G6PDH activity was significantly increased over time and greater as compared with the controls. Thus, DNA damage blocked GAPDH and PYK activities, but strongly enhanced G6PDH activity. Moreover, MMS treatment did not seem to affect the affinity ($K_m$) of GAPDH, PYK, and G6PDH for their specific substrates as compared with non-treatment (controls, Fig. 4). The affinity for specific substrate varied from this enzyme to others. In many cases, MMS reduced the affinity (increased $K_m$), while they promoted affinity (decreased $K_m$) in other cases (Fig. 1).

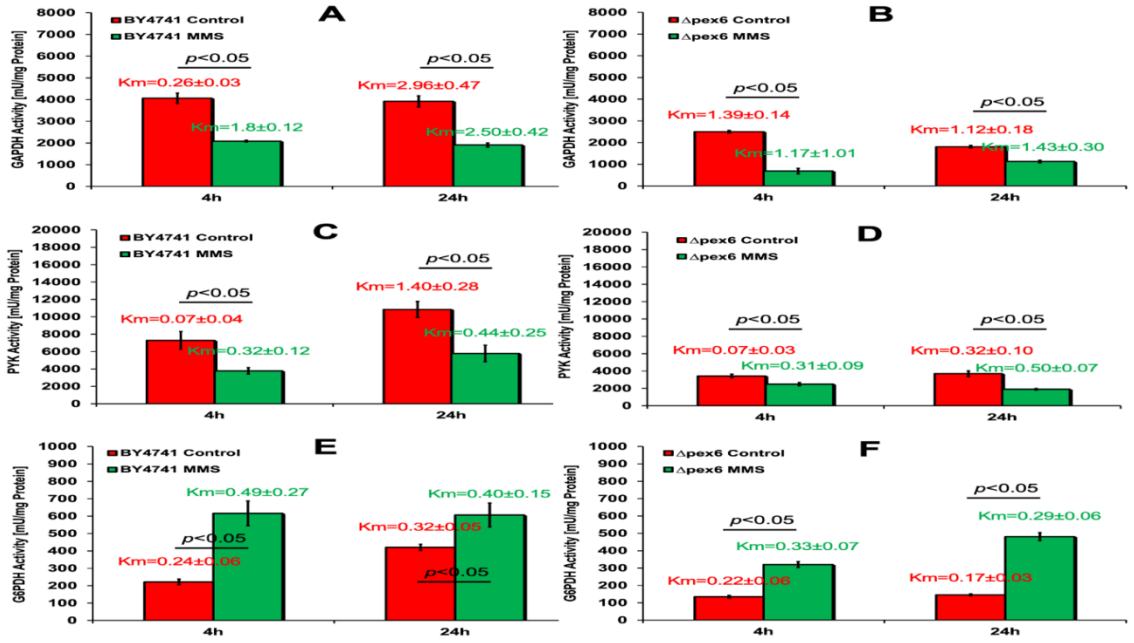


*Figure 1*. Changes in activity of glycolytic enzymes of BY4741 and Δpex6 in response to DNA damage. Protein isolation (cell lysate) was introduced to an enzymatic assay for determination of enzyme activity and Michaelis-Menten constants, $V_{max}$ and $K_m$. Graphs represent activity of GAPDH (A, B), PYK (C, D) and G6PDH (E, F) expressed by $V_{max}$ in mU/mg protein and together with $K_m$ in mM. Results are given as mean values with standard deviations (SD). The differences between the means were analyzed by one-way ANOVA, *p*-value < 0.05 was considered to be significantly different and vice versa

**Inhibition of mitochondrial activity upon MMS treatment**

Also, MMS treatment caused gradually increasing repression of mitochondrial activity of all cultures over the cultivation period (Fig. 2). Additionally, the mitochondrial activity of the control cells was gradually decreased, but that of MMS-treated cells decreased faster than the controls ($p < 0.05$; Fig. 1C). Certainly, the mitochondrial activity of the wild type BY4741 cells was higher than that of the mutant cells in both control and MMS-treated conditions ($p < 0.05$; Fig. 1C). Thus, disruption of the *PEX6* gene leads to the inhibition of mitochondrial activity upon either treatment or non-treatment with MMS.

**Changes in oxygen consumption and metabolite production upon MMS treatment**

Oxygen consumption and cell growth expressed in the percentage of oxygen saturation and $OD_{600}$, respectively, were represented in Figure 3. The results show that MMS caused adverse impairment of mitochondrial respiration leading to a strong inhibition of oxygen consumption and cell growth at all MMS investigated concentrations, especially for the mutant Δ*pex6* cells. MMS treatment significantly diminished oxygen consumption and cell proliferation in a dose-dependent manner (Figs 3 A–B). Then, mitochondrial respiration was either recovered until oxygen in the medium became exhausted or remained inhibited, the lower the MMS concentrations treated, the faster the mitochondrial respiration recovered (Figs 3 A–B). The mutant Δ*pex6* cells were much more sensitive to MMS treatment and demonstrated a stronger enhancement of mitochondrial respiratory block resulting in a more rapid decrease of oxygen consumption as compared

with the wild types (Fig. 3A). Consequently, the mutant cells were not able to recover cell proliferation when exposed to genotoxic chemical as the wild type could (Fig. 3B).

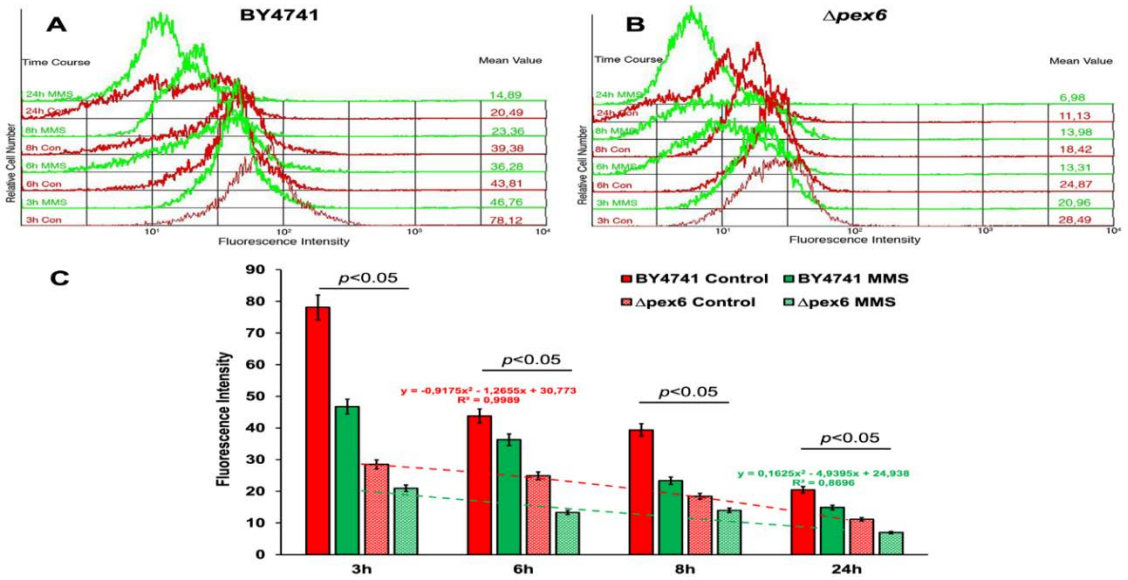


*Figure 2*. Modulation of mitochondrial activity of BY4741 (A) and Δ*pex6* (B) in response to DNA damage. Fluorescence intensity of MitoTracker® was quantified and analyzed by FACS for measuring mitochondrial activity. A and B are kinetic graphs displayed as overlapping histograms of fluorescence intensity against relative cell number. The dashed lines with quadratic equations represent the trends of mitochondrial activity during 24 hours of cultivation (C). Results are given as mean values with standard deviations (SD). The differences between the means were analyzed by one-way ANOVA, *p*-value < 0.05 was considered to be significantly different and vice versa

**Changes in ATP production and UDP-NacGlu synthesis upon MMS treatment**

As shown in Figure 3, MMS treatment prohibited ATP synthesis of both the wild type and Δ*pex6* already after 3 h of treatment resulting in reduction of ATP levels as compared with the controls (Fig. 3C). Moreover, the wild type BY4741 cells produced more ATP levels than the mutant Δ*yca1* cells in either control or MMS-treated condition. Generally, the ATP production was gradually decreased until the end of the cultivation period (Fig. 3C).

In contrast to that, MMS treatment enhanced the synthesis of uridine-diphosphoglucose-N-acetylglucosamine (UDP-NacGlu) in both BY4741 and particularly Δ*pex6* cultures, i.e. the biosynthesis of UDP-NacGlu in the Δ*pex6* cells was much more increased than that in the BY4741 (Fig. 3D). Namely, UDP-NacGlu level of both MMS-treated cultures tended to increase and reached the maximum level at 8 h, then UDP-NacGlu content remained at high level until 24 hours of cultivation, while that of the control cultures was slightly increased around 3 h, then started to decrease over time (Fig. 3D).

**Glycogen and trehalose accumulation upon MMS treatment**

The findings illustrated in Figure 4 reveal that all control cultures did not accumulate glycogen over time while consuming glucose in the medium (Figs. 4A–B). In opposition, all MMS-treated cultures started to accumulate glycogen already when the glucose still remained in the medium and promoted

glycogen accumulation intensively until glucose completely exhausted in the medium (Figs. 4A–B). Maximum glycogen accumulations were reached at around 6 h of cultivation in both the MMS-treated cultures. In addition, the maximum glycogen level of Δ*pex6* was significantly higher than that of the wild type, and composed of up to 9% of cell dry weight (DW) while that of the wild type constituted 4% of DW (Fig. 4A).

Similar to glycogen, all MMS-treated cells accumulated trehalose even though the glucose remained in the medium (Figs. 4C–D). Also, maximum trehalose levels were reached at about 6 h in both the MMS-treated cells. However, all control cultures of BY4741 and Δ*pex6* started to accumulate trehalose from the beginning of cultivation and kept accumulating until glucose was completely exhausted in the medium. And again, the trehalose level of Δ*pex6* was obviously greater and made up 13% DW as compared with that of the BY4741 was 3% DW (Figs. 4C–D). Furthermore, the Δ*pex6* cells accelerated trehalose accumulation over time and up to 24 h of cultivation (Fig. 4C).

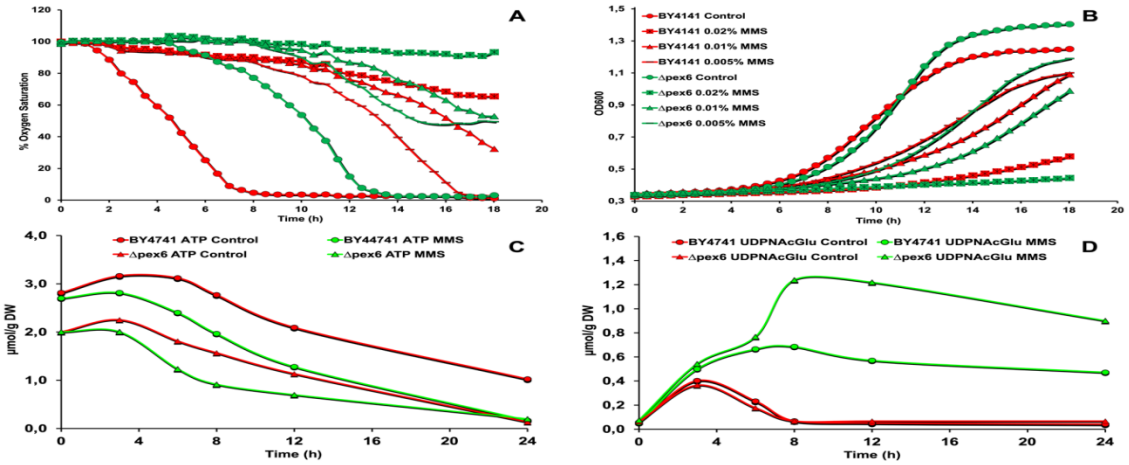


*Figure 3*. Kinetics and changes in oxygen consumption (A), cell growth (B), ATP (C) and UDP-NAcGlu (D) synthesis of the wild type BY4741 and mutant Δ*pex6* in response to DNA damage. Oxygen consumption (% oxygen saturation) and cell growth ($OD_{600}$) were monitored in 96-well OxoPlate®. The legends in $OD_{600}$ (B) are also ones in % oxygen saturation (A). Intracellular metabolite extracts were analyzed by HPIC. The value of ATP and UDP-NAcGlu (uridine-diphosphoglucose-*N*-acetylglucosamine) contents was calculated in µmol/g DW (dry weight, panels C, D)

**Induction of necrosis upon MMS treatment**

Taking into account the principle, annexin V binds to phosphatidylserine that is translocated from the inner to the outer cell membrane layer during apoptosis and PI only enters cells with damaged membrane. Apoptosis stages and apoptotic cell ratios were determined by annexin V/PI double staining and represented in Figure 5. MMS treatment not only reduced the relative cell number, i.e. increased the percentage of apoptotic cells, but also caused an increase in the population of cells in early apoptosis (V+/PI–), late apoptosis (V+/PI+), and necrosis (V–/PI+) as compared with the controls ($p < 0.05$; Fig. 5). In general, the living cells were gradually decreased, whereas the early, late apoptotic, and necrotic cells were consistently increased. In addition, the relative cell number of the mutant Δ*pex6* was significantly less than

that of the wild type BY4741, while the necrotic cells of the mutant were remarkably higher than those of the wild type ($p < 0.05$; Fig. 5).

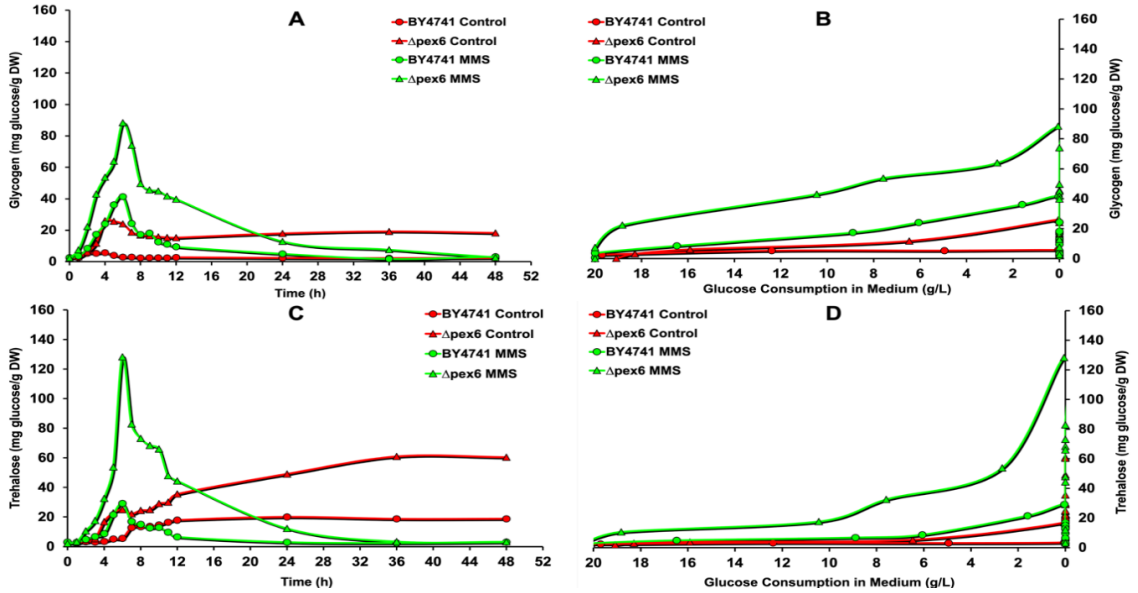


Figure 4. Modulation of glycogen and trehalose accumulation in response to DNA damage. Supernatants were used for monitoring glucose consumption by the Gloxo Assay. Pellets were used for quantifying glycogen and trehalose contents by the Glycogen and Trehalose Assay. The kinetics of glycogen and trehalose accumulation against time of cultivation was depicted in A and C, respectively, while glycogen and trehalose accumulation in mg glucose/g DW against glucose consumption in g/L medium were represented in B and D, respectively

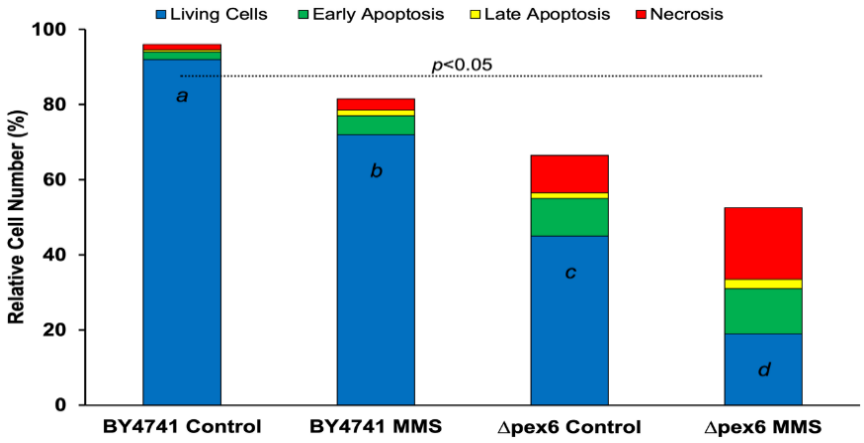


*Figure 5*. Induction of apoptosis and necrosis in BY4741 and Δ*pex6* cells in response to DNA damage. Apoptosis stages and apoptotic cell ratios (%) were determined by FACS flow cytometry using annexin V/PI double staining and calculated by hemacytometer using trypan blue staining, respectively. All measurements were performed at least 3 times for reproducibility and values are means of 3 measurements. The differences between the means were analyzed by Duncan's Multiple Range Test and one-way ANOVA, means with the same letter are not significantly different ($p > 0.05$) and vice versa

## DISCUSSION

### Modulation of glycolytic enzymes in response to DNA damage

As already mentioned, glycolytic enzymes play a crucial role in oxidative stress and apoptosis. The diversion of metabolic flux depends on their activity. Indeed, DNA damage strongly inhibited the activity of two key glycolytic enzymes, GAPDH and PYK, but enhanced that of G6PDH (Fig. 1).

G6PDH (glucose-6-phosphate dehydrogenase) catalyzes the first step in the pentose phosphate pathway (PPP) that produces NADPH. This reductant and reduced glutathione (GSH) are essential in many biosynthetic pathways and protect the cell from endogenous oxidative damage like reactive oxygen species (ROS) or exogenous DNA damaging chemicals (Berg et al., 2002). Moreover, it was stated that G6PDH has a relevant role in the defense mechanism against oxidative stress in bacteria, yeast, and mammalian cells and also suggested that G6PDH as an antioxidative enzyme can be included in the group of catalase, superoxide dismutase, ascorbate peroxidase, and glutathione reductase/peroxidase (Lapshina et al., 2006; Valderrama et al., 2006).

GAPDH (or triose phosphate dehydrogenase - TDH, in yeast) catalyzes the generation of 1,3-diphosphoglycerate from glyceraldehyde-3-phosphate in the sixth step of the glycolytic pathway. GAPDH acts as a reversible metabolic switch under cellular oxidative stress. When cells are exposed to the oxidants, they require excessive amounts of the antioxidant cofactor NADPH. Oxidant treatment causes an inactivation of GAPDH, but activation of G6PDH. This effect re-routes temporarily the metabolic flux from glycolysis to the PPP, allowing the cell to produce more NADPH for antioxidant systems (Hara et al., 2006; Ralser et al., 2007).

Regarding pyruvate kinase (PYK), to our knowledge, there has been no report of the role of yeast PYK in oxidative defence systems or apoptosis so far. However, many studies have been reported about the role of PYK in oxidative defence systems of mammalian cells and human tumors (Liang et al., 2017; Matte et al., 2021; Prakasam et al., 2017; Wu et al., 2021), though our own previous research indicated that high ROS accumulation strongly inhibits the activity of GAPDH and PYK, but enhances that of G6PDH upon MMS treatment in *S. cerevisiae* (Kitanovic et al., 2009).

Thus, DNA damage is responsible for the inhibition of GAPDH and PYK activities but enhancement of G6PDH activity that could lead to a subsequent repression of mitochondrial activity.

### Modulation of mitochondrial activity in response to DNA damage

Because the later stage of glycolysis was suppressed as a result of inhibited GAPDH and PYK activities (Figs. 1A–D), this effect led to a reduced mitochondrial activity of all cells, especially the Δ*pex6* cells in both conditions with or without MMS treatment (Fig. 2).

Probably, the reduced mitochondrial activity results from mitochondrial DNA (mtDNA) damage triggered by MMS treatment that induces high ROS accumulation and further impairs mitochondrial activity. Since mtDNA might be more prone to oxidative damage and suffers 3–10 fold more damage than nuclear DNA (nDNA) in numerous cell types from yeast, mouse, rats, and humans (Chenna et al., 2022; Van Houten et al., 2006). Moreover, ROS can be generated from both exogenous and endogenous pathways and even during normal metabolism, and pose a significant damage to DNA, lipids, and protein (Mendelow, 2009; Salmon et al., 2004). Recently, role of yeast *HAP4* gene in mitochondrial function, oxidative phosphorylation, and apoptosis in response to DNA damage (Bui & Nguyen, 2025). Thus, it could be suggested that cells lacking Pex6 (peroxisomal biogenesis factor 6) led to a reduced mitochondrial activity regardless of MMS treatment and subsequent inhibition of cell growth that shoud be discussed later.

**Modulation of oxygen consumption and metabolite production in response to DNA damage**

The above results explain that DNA damage strongly inhibits the activity of GAPDH and PYK and mitochondrial activity that could lead to decreased oxygen consumption and cell growth, especially for the Δ*pex6* cells. Undoubtedly, cells defective in the *PEX6* gene led to inhibited oxygen saturation and exponential growth rate as compared with the wild type (Figs. 3A–B). Whereas, as result from high mitochondrial activity, the wild type was able to recover mitochondrial respiration and oxygen consumption faster and increase cell survival better than the mutant (Fig. 2 & Figs. 3A–B). Possibly, the low mitochondrial activity together with oxygen consumption could result from mtDNA damage triggered by MMS treatment that induces high ROS accumulation as discussed above.

Thus, low oxygen consumption and mitochondrial activity led to an impairment of ATP synthesis in MMS-treated and even MMS-untreated Δ*pex6* cells (Fig. 3C). Surprisingly, both UDP-NacGlu synthesis (Fig. 3D) and G6PDH activity (Figs. 1E–F) were more progressively enhanced in MMS-treated cells, especially for the MMS-treated Δ*pex6* cells. It is documented that UDP-NacGlu produced in the hexosamine biosynthesis pathway (HBP) serves as a substrate for most glycosylation pathways, and is used to glycosylate proteins known as O-linked and N-linked glycosylation that play an important role in cellular signaling (Halim et al., 2015; Vigetti et al., 2014). It is speculated that when the final steps of glycolysis and the ATP synthesis are blocked, metabolic flux (glucose) does not enter to the TCA cycle and further to the respiratory chain, but to the pentose phosphate pathway (PPP) as a result of increased G6PDH activity and probably to glycogen/trehalose syntheis because of enhanced UDP-NacGlu synthesis.

**Modulation of glycogen and trehalose synthesis in response to DNA damage**

As expected, all MMS-treated cells, especially the mutant Δ*pex6* cells, promoted the glycogen and trehalose synthesis more intensively than the control cells in response to DNA damage (Fig. 4). This means that the carbohydrate flux was diverted not only to the PPP and HBP, but also to glycogen and trehalose synthesis that yeast cells utilize as major energy reserves to maintain their energy and survival.

These findings suggest that the control cells were able to metabolize by-products such as glycerol or non-fermentative carbon from glucose fermentation through aerobic metabolism and could supply their energy over time until the nutrients are depleted in the medium. Whereas, MMS-treated cells were not able to switch from fermentative to respiratory metabolism whereby they could utilize non-fermentative products, they started to mobilize their reserve carbohydrates in the form of glycogen and trehalose and ran out of these reserve carbohydrates more rapidly (Figs. 4A–C).

These results are in agreement with the supposition that glycogen and trehalose synthesis correlate with the survival of yeast cells in response to different stress conditions (Parrou et al., 1997; Virgilio et al., 2017). Also, glycogen and trehalose can be broken down yielding glucose molecules that yeast cells could rely on and utilize to maintain their energy in response to physico-chemical stresses (Francois & Parrou, 2001; Gomes et al., 2020; Virgilio et al., 2017). Moreover, these findings also fit our previous observation in other yeast cells of the FF 18984 strain (Kitanovic et al., 2009).

**Induction of necrosis in response to DNA damage**

It has been recognized that mitochondria play a central role in the energy metabolism, respiratory chain, and apoptosis (Nadalutti et al., 2020; Van Houten et al., 2006). Also, they function as “executioners” in programmed cell death (apoptosis). Definitely, DNA damage contributed to the activation of apoptosis (Huang et al., 2021; Kwun & Lee, 2020; X. Wang et al., 2021). As above indicated, DNA damage impaired the mitochondrial respiration

and energy metabolism of all cells (Figs. 2, 3) that could lead to the induction of apoptosis as a cellular defense mechanism in response to DNA damage.

As anticipated, the living cells were progressively decreasing, while the early, late apoptotic, and particularly necrotic cells were steadily increasing. Deletion of *PEX6* gene led to reduction of the living cells but increment of apoptotic cells, especially necrotic cells (Fig. 5). Since cells lacking *PEX6* gene lead to loss of cell viability and cause necrotic cell death (Jungwirth et al., 2008). These results suggest that fully functional peroxisomal biogenesis factor 6 (Pex6) plays a major role in cell proliferation and cellular defense mechanism in response to DNA damage.

However, Pex1 is also an important component of the Pex1/Pex6 complex. This complex regulates the peroxisomal matrix protein import, peroxisomal receptor recycling, and peroxisome formation (Ali et al., 2023; Grimm et al., 2012; Rüttermann et al., 2023). Maybe, Pex1 interacts with Pex6 to fulfil their role in such functions. Moreover, there are 10 enzymes which catalyse the steps of glycolysis. Of which are hexokinase, phosphoglucose isomerase, phosphofructokinase, phosphoglyceromutase, etc., whose activity certainly impacts glucose flux. Additionally, Mig1 encoded by *MIG1* binds to the Hxk2/Snf1 complex that inhibits genes involved in respiration, gluconeogenesis, and alternative carbon source utilization. Deficiency in *MIG1* leads to a decrease of mitochondrial respiration and loss of control in glucose utilization (Schüller, 2003; Peeters & Thevelein, 2014), and presumably diverts glucose flux to glycogen and trehalose synthesis. Nonetheless, these assumptions and issues remain unsettled and are also the limitations of this study, they should therefore be considered in our further studies.

## CONCLUSION

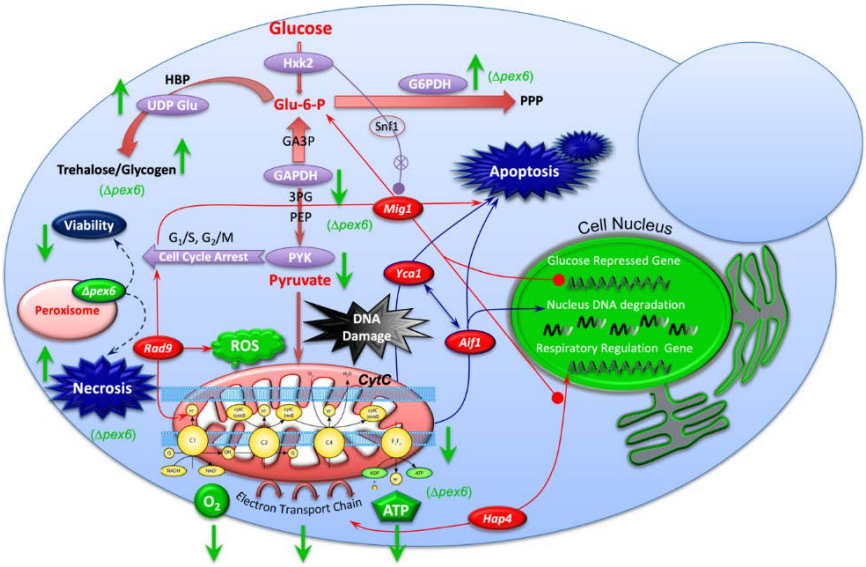


*Figure 6*. Schematic summary of the role of the yeast *PEX6* gene in glycolysis, mitochondrial respiration, ATP synthesis, glycogen/trehalose accumulation, and necrosis in response to DNA damage (see text for details)

MMS, an alkylating agent and carcinogen, methylates the $N^7$-deoxyguanine and $N^3$-deoxyadenine bases of DNA, directly causing double-strand breaks and stalling replication forks (Groth et al., 2010; Yang et al., 2010). As a consequence, DNA damage caused a prohibition of activity of GAPDH and PYK, as well as mitochondrial respiration, cell

growth, and ATP synthesis, while it simultaneously intensely enhanced the G6PDH activity and UDP-NacGlu synthesis. Subsequently, the glucose flux was deviated to the PPP as a result of increased G6PDH activity and to glycogen/trehalose synthesis because of enhanced levels of UDP-NacGlu . The cells, especially the mutant Δ*pex6*, utilize glycogen/trehalose as their major energy reserves to maintain their energy and survival, and induced necrosis as a cellular defense mechanism in response to DNA damage (Fig. 6).

***Acknowledgements:*** We thank Stefan Wölfl, Ana Kitanovic for valuable comments regarding the experiments and sharing ideas regarding data analysis. This work was supported by the SysMO Project Network (EU-BMBF) on Systems Biology of Microorganisms (MOSES, WP 4.3, S.W. and A.K.).

## REFERENCES

Ali B. A., Judy R. M., Chowdhury S., Jacobsen N. K., Castanzo D. T., Carr K. L., Richardson C. D., Lander G. C., Martin A., Gardner B. M., 2023. The Pex6 N1 domain is required for Pex15 binding and proper assembly with Pex1. *bioRxiv*. https://doi.org/10.1101/2023.09.15.557798

Berg J. M., Tymoczko J. L., Stryer L., 2002. *Biochemistry, Fifth Edition*: W.H. Freeman.

Bonowski F., Kitanovic A., Ruoff P., Holzwarth J., Kitanovic I., Bui V. N., Lederer E., Wolfl S., 2010. Computer controlled automated assay for comprehensive studies of enzyme kinetic parameters. *PLoS One,* 5(5): e10727. doi: 10.1371/journal.pone.0010727

Bui V. N., & Nguyen D. H., 2025. Role of yeast *HAP4* gene in mitochondrial function, oxidative phosphorylation, and apoptosis in response to DNA damage. *Academia Journal of Biology*, *47*(1): 111–125. https://doi.org/10.15625/2615-9023/21232

Bui V. N., Nguyen T. P. T., Nguyen H. D., Phi Q. T., Nguyen T. N., Chu H. H., 2024. Bioactivity responses to changes in mucus-associated bacterial composition between healthy and bleached Porites lobata corals. *J Invertebr Pathol*, 206: 108164. doi: 10.1016/j.jip.2024.108164

Cerella C., D'Alessio M., Cristofanon S., De Nicola M., Radogna F., Dicato M., Diederich M., Ghibelli L., 2009. Subapoptogenic oxidative stress strongly increases the activity of the glycolytic key enzyme glyceraldehyde 3-phosphate dehydrogenase. *Ann N Y Acad Sci*, 1171: 583−590. https://doi.org/10.1111/j.1749-6632.2009.04723.x

Chenna S., Koopman W. J. H., Prehn J. H. M., Connolly N. M. C., 2022. Mechanisms and mathematical modeling of ROS production by the mitochondrial electron transport chain. *Am J Physiol Cell Physiol*, 323(1): C69-C83. https://doi.org/10.1152/ajpcell.00455.2021

Christodoulou D., Link H., Fuhrer T., Kochanowski K., Gerosa L., Sauer U., 2018. Reserve Flux Capacity in the Pentose Phosphate Pathway Enables Escherichia coli's Rapid Response to Oxidative Stress. *Cell Syst*, 6(5): 569−578. https://doi.org/10.1016/j.cels.2018.04.009

Ebberink M. S., Kofster J., Wanders R. J., Waterham H. R., 2010. Spectrum of PEX6 mutations in Zellweger syndrome spectrum patients. *Hum Mutat*, 31(1): E1058−1070. https://doi.org/10.1002/humu.21153

Francois J., & Parrou J. L., 2001. Reserve carbohydrates metabolism in the yeast Saccharomyces cerevisiae. *FEMS Microbiol Rev*, 25(1): 125−145. https://doi.org/10.1111/j.1574-6976.2001.tb00574.x

Geisbrecht B. V., Collins C. S., Reuber B. E., Gould S. J., 1998. Disruption of a PEX1-PEX6 interaction is the most common cause of the neurologic disorders Zellweger syndrome, neonatal adrenoleukodystrophy, and infantile Refsum disease. *Proc Natl Acad Sci U S A*, 95(15): 8630−8635. https://doi.org/10.1073/pnas.95.15.8630

Gomes A. M. V., Orlandi A., Parachin N. S., 2020. Deletion of the trehalose tps1 gene

in Kluyveromyces lactis does not impair growth in glucose. *FEMS Microbiol Lett*, 367(10). doi: 10.1093/femsle/fnaa072

Grimm I., Saffian D., Platta H. W., Erdmann R., 2012. The AAA-type ATPases Pex1p and Pex6p and their role in peroxisomal matrix protein import in Saccharomyces cerevisiae. *Biochim Biophys Acta*, 1823(1): 150−158. https://doi.org/10.1016/j.bbamcr.2011.09.005

Groth P., Auslander S., Majumder M. M., Schultz N., Johansson F., Petermann E., Helleday T., 2010. Methylated DNA causes a physical block to replication forks independently of damage signalling, O(6)-methylguanine or DNA single-strand breaks and results in DNA damage. *J Mol Biol*, 402(1): 70−82. https://doi.org/10.1016/j.jmb.2010.07.010

Grüning N. M., Rinnerthaler M., Bluemlein K., Mülleder M., Wamelink M. M., Lehrach H., Jakobs C., Breitenbach M., Ralser M., 2011. Pyruvate kinase triggers a metabolic feedback loop that controls redox metabolism in respiring cells. *Cell Metab*, 14(3): 415−427. https://doi.org/10.1016/j.cmet.2011.06.017

Halim A., Larsen I. S., Neubert P., Joshi H. J., Petersen B. L., Vakhrushev S. Y., Strahl S., Clausen H., 2015. Discovery of a nucleocytoplasmic O-mannose glycoproteome in yeast. *Proc Natl Acad Sci U S A*, 112(51): 15648−15653. https://doi.org/10.1073/pnas.1511743112

Hara M. R., Thomas B., Cascio M. B., Bae B. I., Hester L. D., Dawson V. L., Dawson T. M., Sawa A., Snyder S. H., 2006. Neuroprotection by pharmacologic blockade of the GAPDH death cascade. *Proc Natl Acad Sci U S A*, 103(10): 3887–3889. https://doi.org/10.1073/pnas.0511321103

Hildebrandt T., Knuesting J., Berndt C., Morgan B., Scheibe R., 2015. Cytosolic thiol switches regulating basic cellular functions: GAPDH as an information hub? *Biol Chem*, 396(5): 523−537. https://doi.org/10.1515/hsz-2014-0295

Huang Y. L., Pan W. L., Cai W. W., Ju J. Q., Sun S. C. 2021. Exposure to citrinin induces DNA damage, autophagy, and mitochondria dysfunction during first cleavage of mouse embryos. *Environ Toxicol*, 36(11): 2217−2224. https://doi.org/10.1002/tox.23335

Jungwirth H., Ring J., Mayer T., Schauer A., Büttner S., Eisenberg T., Carmona-Gutierrez D., Kuchler K., Madeo F., 2008. Loss of peroxisome function triggers necrosis. *FEBS Lett*, 582(19): 2882−2886. doi: 10.1016/j.febslet.2008.07.023

Kitanovic A., Walther T., Loret M. O., Holzwarth J., Kitanovic I., Bonowski F., Van Bui N., Francois J. M., Wolfl S., 2009. Metabolic response to MMS-mediated DNA damage in Saccharomyces cerevisiae is dependent on the glucose concentration in the medium. *FEMS Yeast Res*, 9(4): 535−551. https://doi.org/10.1111/j.1567-1364.2009.00505.x

Kwun M. S., & Lee D. G., 2020. Quercetin-induced yeast apoptosis through mitochondrial dysfunction under the accumulation of magnesium in Candida albicans. *Fungal Biol*, 124(2): 83−90. doi: 10.1016/j.funbio.2019.11.009

Lapshina E. A., Sudnikovich E. J., Maksimchik J. Z., Zabrodskaya S. V., Zavodnik L. B., Kubyshin V. L., Nocun M., Kazmierczak P., Dobaczewski M., Watala C., Zavodnik I. B., 2006. Antioxidative enzyme and glutathione S-transferase activities in diabetic rats exposed to long-term ASA treatment. *Life Sci*, 79(19): 1804−1811. https://doi.org/10.1016/j.lfs.2006.06.008

Liang J., Cao R., Wang X., Zhang Y., Wang P., Gao H., Li C., Yang F., Zeng R., Wei P., Li D., Li W., Yang W., 2017. Mitochondrial PKM2 regulates oxidative stress-induced apoptosis by stabilizing Bcl2. *Cell Res*, 27(3): 329−351. https://doi.org/10.1038/cr.2016.159

Loret M. O., Pedersen L., François J., 2007. Revised procedures for yeast metabolites extraction: application to a glucose pulse

to carbon-limited yeast cultures, which reveals a transient activation of the purine salvage pathway. *Yeast*, 24(1): 47−60. https://doi.org/10.1002/yea.1435

Lucaccioni L., Righi B., Cingolani G. M., Lugli L., Della Casa E., Torcetta F., Iughetti L., Berardi A., 2020. Overwhelming sepsis in a neonate affected by Zellweger syndrome due to a compound heterozygosis in PEX 6 gene: a case report. *BMC Med Genet*, 21(1): 229. doi: 10.1186/s12881-020-01175-y

Matte A., Federti E., Kung C., Kosinski P. A., Narayanaswamy R., Russo R., Federico G., Carlomagno F., Desbats M. A., Salviati L., Leboeuf C., Valenti M. T., Turrini F., Janin A., Yu S., Beneduce E., Ronseaux S., Iatcenko I., Dang L., Ganz T., Jung C. L., Iolascon A., Brugnara C., De Franceschi L., 2021. The pyruvate kinase activator mitapivat reduces hemolysis and improves anemia in a β-thalassemia mouse model. *J Clin Invest*, 131(10). https://doi.org/10.1172/jci144206

Mendelow B. V. (2008). *Molecular medicine for clinicians*. Johannesburg, South Africa: Wits University Press.

Min K., Son H., Lee J., Choi G. J., Kim J. C., Lee Y. W., 2012. Peroxisome function is required for virulence and survival of Fusarium graminearum. *Mol Plant Microbe Interact*, 25(12): 1617−1627. https://doi.org/10.1094/mpmi-06-12-0149-r

Muronetz V. I., Melnikova A. K., Saso L., Schmalhausen E. V., 2020. Influence of Oxidative Stress on Catalytic and Non-glycolytic Functions of Glyceraldehyde-3-phosphate Dehydrogenase. *Curr Med Chem*, 27(13): 2040−2058. https://doi.org/10.2174/0929867325666180530101057

Nadalutti C. A., Stefanick D. F., Zhao M. L., Horton J. K., Prasad R., Brooks A. M., Griffith J. D., Wilson S. H., 2020. Mitochondrial dysfunction and DNA damage accompany enhanced levels of formaldehyde in cultured primary human fibroblasts. *Sci Rep*, 10(1): 5575. doi: 10.1038/s41598-020-61477-2

Parrou J. L., Teste M. A., Francois J., 1997. Effects of various types of stress on the metabolism of reserve carbohydrates in Saccharomyces cerevisiae: genetic evidence for a stress-induced recycling of glycogen and trehalose. *Microbiology (Reading)*, 143 ( Pt 6): 1891−1900. doi: 10.1099/00221287-143-6-1891

Prakasam G., Singh R. K., Iqbal M. A., Saini S. K., Tiku A. B., Bamezai R. N. K., 2017. Pyruvate kinase M knockdown-induced signaling via AMP-activated protein kinase promotes mitochondrial biogenesis, autophagy, and cancer cell survival. *J Biol Chem*, 292(37): 15561−15576. https://doi.org/10.1074/jbc.M117.791343

Ralser M., Wamelink M. M., Kowald A., Gerisch B., Heeren G., Struys E. A., Klipp E., Jakobs C., Breitenbach M., Lehrach H., Krobitsch S., 2007. Dynamic rerouting of the carbohydrate flux is key to counteracting oxidative stress. *J Biol*, 6(4): 10. https://doi.org/10.1186/jbiol61

Renaud M., Guissart C., Mallaret M., Ferdinandusse S., Cheillan D., Drouot N., Muller J., Claustres M., Tranchant C., Anheim M., Koenig M., 2016. Expanding the spectrum of PEX10-related peroxisomal biogenesis disorders: slowly progressive recessive ataxia. *J Neurol*, 263(8): 1552−1558. https://doi.org/10.1007/s00415-016-8167-3

Ritter J. B., Genzel Y., Reichl U., 2006. High-performance anion-exchange chromatography using on-line electrolytic eluent generation for the determination of more than 25 intermediates from energy metabolism of mammalian cells in culture. *J Chromatogr B Analyt Technol Biomed Life Sci*, 843(2): 216−226. https://doi.org/10.1016/j.jchromb.2006.06.004

Rüttermann M., Koci M., Lill P., Geladas E. D., Kaschani F., Klink B. U., Erdmann R., Gatsogiannis C., 2023. Structure of the peroxisomal Pex1/Pex6 ATPase complex bound to a substrate. *Nat Commun*, 14(1):

5942. https://doi.org/10.1038/s41467-023-41640-9

Salmon T. B., Evert B. A., Song B., Doetsch P. W., 2004. Biological consequences of oxidative stress-induced DNA damage in Saccharomyces cerevisiae. *Nucleic Acids Res,* 32(12): 3712−3723. https://doi.org/10.1093/nar/gkh696

Shimizu K., & Matsuoka Y., 2019. Redox rebalance against genetic perturbations and modulation of central carbon metabolism by the oxidative stress regulation. *Biotechnol Adv,* 37(8): 107441. https://doi.org/10.1016/j.biotechadv.2019.107441

Sousa B., Pereira J., Marques R., Grilo L. F., Pereira S. P., Sardão V. A., Schmitt F., Oliveira P. J., Paredes J., 2020. P-cadherin induces anoikis-resistance of matrix-detached breast cancer cells by promoting pentose phosphate pathway and decreasing oxidative stress. *Biochim Biophys Acta Mol Basis Dis,* 1866(12): 165964. doi: 10.1016/j.bbadis.2020.165964

Ueda K., Nakajima T., Yoshikawa K., Toya Y., Matsuda F., Shimizu H., 2018. Metabolic flux of the oxidative pentose phosphate pathway under low light conditions in Synechocystis sp. PCC 6803. *J Biosci Bioeng,* 126(1): 38−43. https://doi.org/10.1016/j.jbiosc.2018.01.020

Valderrama R., Corpas F. J., Carreras A., Gomez-Rodriguez M. V., Chaki M., Pedrajas J. R., Fernandez-Ocana A., Del Rio L. A., Barroso J. B., 2006. The dehydrogenase-mediated recycling of NADPH is a key antioxidant system against salt-induced oxidative stress in olive plants. *Plant Cell Environ,* 29(7): 1449−1459. https://doi.org/10.1111/j.1365-3040.2006.01530.x

Van Houten B., Woshner V., Santos J. H., 2006. Role of mitochondrial DNA in toxic responses to oxidative stress. *DNA Repair (Amst),* 5(2): 145−152. https://doi.org/10.1016/j.dnarep.2005.03.002

Vigetti D., Viola M., Karousou E., De Luca G., Passi A., 2014. Metabolic control of hyaluronan synthases. *Matrix Biol,* 35: 8−13. https://doi.org/10.1016/j.matbio.2013.10.002

Virgilio S., Cupertino F. B., Ambrosio D. L., Bertolini M. C., 2017. Regulation of the reserve carbohydrate metabolism by alkaline pH and calcium in Neurospora crassa reveals a possible cross-regulation of both signaling pathways. *BMC Genomics,* 18(1): 457. https://doi.org/10.1186/s12864-017-3832-1

Wang H., Nicolay B. N., Chick J. M., Gao X., Geng Y., Ren H., Gao H., Yang G., Williams J. A., Suski J. M., Keibler M. A., Sicinska E., Gerdemann U., Haining W. N., Roberts T. M., Polyak K., Gygi S. P., Dyson N. J., Sicinski P., 2017. The metabolic function of cyclin D3-CDK6 kinase in cancer cell survival. *Nature,* 546(7658): 426−430. https://doi.org/10.1038/nature22797

Wang X., Ni H., Xu W., Wu B., Xie T., Zhang C., Cheng J., Li Z., Tao L., Zhang Y., 2021. Difenoconazole induces oxidative DNA damage and mitochondria mediated apoptosis in SH-SY5Y cells. *Chemosphere,* 283: 131160. https://doi.org/10.1016/j.chemosphere.2021.131160

Wu X., Liu L., Zheng Q., Hao H., Ye H., Li P., Yang H., 2021. Protocatechuic aldehyde protects cardiomycoytes against ischemic injury via regulation of nuclear pyruvate kinase M2. *Acta Pharm Sin B,* 11(11): 3553−3566. https://doi.org/10.1016/j.apsb.2021.03.021

Yang Y., Gordenin D. A., Resnick M. A., 2010. A single-strand specific lesion drives MMS-induced hyper-mutability at a double-strand break in yeast. *DNA Repair (Amst),* 9(8): 914−921. https://doi.org/10.1016/j.dnarep.2010.06.005